Targeted deletion of *Sost* distal enhancer increases bone formation and bone mass

Nicole M. Collette[a], Damian C. Genetos[b], Aris N. Economides[c], LiQin Xie[c], Mohammad Shahnazari[d], Wei Yao[d], Nancy E. Lane[d], Richard M. Harland[e], and Gabriela G. Loots[a,f,1]

[a]Physical and Life Sciences Directorate, Lawrence Livermore National Laboratories, Livermore, CA 94550; [b]Department of Anatomy, Physiology, and Cell Biology, School of Veterinary Medicine, University of California, Davis, CA 95616; [c]Regeneron Pharmaceuticals, Tarrytown, NY 10591; [d]Department of Internal Medicine, University of California Davis Medical Center, Sacramento, CA 95817; [e]Department of Molecular and Cell Biology, University of California, Berkeley, CA 94720; and [f]Quantitative and Systems Biology Department, School of Natural Sciences, University of California, Merced, CA 95343

Edited by Eric N. Olson, University of Texas Southwestern Medical Center, Dallas, TX, and approved July 16, 2012 (received for review April 30, 2012)

The Wnt antagonist Sost has emerged as a key regulator of bone homeostasis through the modulation of Lrp4/5/6 Wnt coreceptors. In humans, lack of Sclerostin causes sclerosteosis and van Buchem (VB) disease, two generalized skeletal hyperostosis disorders that result from hyperactive Wnt signaling. Unlike sclerosteosis, VB patients lack *SOST* coding mutations but carry a homozygous 52 kb noncoding deletion that is essential for the transcriptional activation of *SOST* in bone. We recently identified a putative bone enhancer, *ECR5*, in the VB deletion region, and showed that the transcriptional activity of *ECR5* is controlled by Mef2C transcription factor in vitro. Here we report that mice lacking *ECR5* or *Mef2C* through *Col1-Cre* osteoblast/osteocyte-specific ablation result in high bone mass (HBM) due to elevated bone formation rates. We conclude that the absence of the *Sost*-specific long-range regulatory element *ECR5* causes VB disease in rodents, and that Mef2C is the main transcription factor responsible for *ECR5*-dependent *Sost* transcriptional activation in the adult skeleton.

osteocytes

Several rare genetic disorders that interfere with Wnt signaling have provided strong evidence that the "canonical" Wnt signaling pathway is critical in bone (1). The Wnt coreceptor LRP5 has been described as a modulator of bone mass where loss-of-function mutations cause osteoporosis-pseudoglioma syndrome (OPPG) (2), an autosomal recessive disorder characterized by low bone mass and skeletal fragility; conversely, gain-of-function *Lrp5* alleles cause high bone mass (HBM) (3). Similar hyperactive osteoblast activity due to elevated Wnt signaling was observed when Sost, a secreted Wnt inhibitor, was mutated in knockout (KO) mice or in sclerosteosis patients who suffer from generalized hyperostosis (4–6). *Lrp5* gene targeting or *SOST* overexpression in transgenic (TG) mice causes osteopenia (3, 7), whereas TG overexpression of G171V *Lrp5* allelic variant causes HBM, similar to the *Sost* KO phenotypes (4, 8, 9). The recapitulation of the human phenotypes in mouse models supports the conclusion that canonical Wnt signaling plays a critical role in bone metabolism, and points to Sost and Lrp5 as key regulators of bone mass.

The skeletal phenotype describing sclerosteosis patients is similar to what has been documented for van Buchem (VB) disease. Although both VB and sclerosteosis map to the same locus on human chromosome 17 that includes the *SOST* transcript, the Sclerostin transcription unit was not affected in VB. All VB patients examined to date carry a 52-kb noncoding deletion, 35 kb downstream of *SOST* that results in the absence of postnatal *SOST* transcript and protein (10, 11). Although both sclerosteosis and VB are caused by sclerostin deficiency, the VB phenotype is a result of dysregulated *SOST* transcription. To identify the potential transcriptional regulatory elements responsible for *Sost* transcription in bone, we have characterized the expression of a human *SOST* transgene or an engineered allele corresponding to VB in mice. Only the wild-type (WT) *SOST* allele faithfully expressed *SOST* in the adult bone and thereby caused osteopenia, whereas the TG mice carrying the VB deletion allele were indistinguishable from WT (7). Cross-species sequence comparisons combined with in vitro and in vivo enhancer assays identified an evolutionarily conserved candidate enhancer element, termed *ECR5*, that drove reporter expression in UMR-106 cells and in the skeletal anlage of the murine embryo at embryonic day (E) 14.5 (7).

Despite wide interest in the manipulation of Sost as a skeletal anabolic therapy, only a modest amount of data has been generated describing the upstream regulatory pathways responsible for its transcription. We have shown in vitro that *Sost* transcription is controlled by both its proximal promoter and the distal enhancer, *ECR5*. Specifically, *ECR5*, which drives reporter gene expression in mature osteoblastic cells, mediates responsiveness to parathyroid hormone (PTH) (12) and TGF-β (13). PTH suppresses the activity of *ECR5*-luciferase constructs independently of the *SOST* promoter and repression occurs via a myocyte enhancer factor 2 (Mef2)-responsive element (12). Among the four Mef2 family members of transcription factors (Mef2A–D), only Mef2C and Mef2D were shown to be robustly expressed in mineralized bone (14), and we determined that Mef2C and Sost colocalize in UMR-106 cells and mouse osteocytes (12). The activity of *ECR5* enhancer was increased by exogenous Mef2C and was inhibited by dominant-negative Mef2C cotransfection. Finally, siRNA-mediated knockdown of *Mef2C–D* significantly suppressed endogenous *Sost* expression (12). Together, these results identified Mef2C as a transcriptional regulatory protein in bone, and position it upstream of *Sost* as a critical transcriptional modulator of the *ECR5* candidate enhancer to control bone-specific *Sost* expression.

In this study, we extend our in vitro results using TG and KO mice. We show that *ECR5* is sufficient to drive TG reporter expression in osteocytes, in adult mice. We also show that targeted deletion of *ECR5* reduces tissue-specific expression of *Sost*, increasing bone formation rates and causing HBM. As in VB patients, the hyperostosis in *ECR5* KO mice ($ECR5^{KO}$) is milder than observed in sclerosteosis patients and murine *Sost* KO models, suggesting that the 338-bp *ECR5* noncoding deletion is sufficient to recapitulate the phenotypes observed in VB disease. Using a combination of *Mef2C;Col1-Cre* and *Mef2C;Col1-Cre;ECR5*-TG compound mice, we show that *ECR5*-mediated osteocyte expression of *Sost* is dependent on Mef2C. In addition,

Author contributions: G.G.L. designed research; N.M.C., D.C.G., L.X., M.S., and W.Y. performed research; D.C.G., A.N.E., and R.M.H. contributed new reagents/analytic tools; N.M.C., W.Y., N.E.L., R.M.H., and G.G.L. analyzed data; and N.M.C., N.E.L., R.M.H., and G.G.L. wrote the paper.

The authors declare no conflict of interest.

This article is a PNAS Direct Submission.

Freely available online through the PNAS open access option.

[1]To whom correspondence should be addressed. E-mail: loots1@llnl.gov.

This article contains supporting information online at www.pnas.org/lookup/suppl/doi:10.1073/pnas.1207188109/-/DCSupplemental.

targeted ablation of *Mef2C* in osteoblasts and osteocytes also causes HBM, indicating that Mef2C is a critical regulatory protein in bone and controls *Sost* expression via *ECR5*, by functioning as a modulator of Wnt signaling and bone homeostasis. As such, the discovery and characterization of the Mef2C-Sclerostin transcriptional axis has important implications for the anabolic treatment of disorders in which bone loss is a significant component.

Results

***ECR5* Drives Transgenic Reporter Expression in Osteoblasts and Osteocytes.** To determine whether *ECR5* functions as a tissue-specific enhancer in vivo, we generated two *ECR5* TG constructs (Fig. 1 *A* and *B*). *ECR5L* included a 2-kb *ECR5* fragment upstream of the mouse β-*globin* minimal promoter driving β-galactosidase (*LacZ*) (Fig. 1*B; ECR5*^{LacZ}). *3XECR5s* included three tandem copies of a 255bp *ECR5* fragment upstream of the 2kb *SOST* promoter driving topaz-green fluorescent protein (*tpzGFP*) (Fig. 1*B*; *3XECR5*^{GFP}). *ECR5*^{LacZ} expression was compared to *Sost*^{LacZ} (*LacZ* replaced *Sost* in *Sost*^{KO}) and was found throughout the skeleton (Fig. 1 *C–F*). In a minority of *ECR5*^{LacZ} lines, TG expression was also observed in the vasculature and the kidney (Fig. 1 *E* and *G*). We also observed kidney expression in *3XECR5*^{GFP} but no expression in the vasculature.

In neonatal calvaria, *ECR5*^{LacZ} (Fig. 1*H*) and *3XECR5*^{GFP} (Fig. 1*I*) expression highlighted osteoblasts and osteocytes, and was indistinguishable from endogenous *Sost* expression (Fig. 1*J*). Both *ECR5*^{LacZ} and *3XECR5*^{GFP} exhibited highly similar skeletal expression pattern in all lines examined (five *ECR5*^{LacZ} and two *3XECR5*^{GFP} lines), with varying degrees of expression intensity. No dramatic differences were noted between *ECR5*^{LacZ} and *3XECR5*^{GFP} expression in the neonatal skeleton, with the exception that *3XECR5*^{GFP} also expressed in hypertrophic chondrocytes. Previously, we also observed TG expression in the hypertrophic chondrocytes of *SOST* TG mice, suggesting that this expression may be specific to the human promoter. These findings allowed us to conclude that the 255-bp *ECR5* element is sufficient to drive osteoblast/osteocyte-specific expression in neonatal mice, independently of the *SOST* promoter. In the adult mice, *3XECR5*^{GFP} expression was more robust in osteocytes than *ECR5*^{LacZ}, suggesting that the *SOST* promoter is also required for high levels of osteocyte-specific expression of *Sost*.

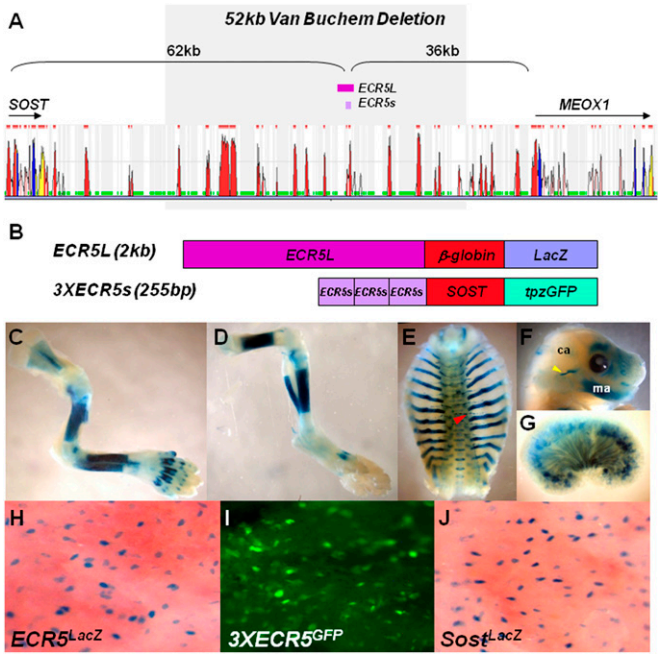

Fig. 1. TG expression of *ECR5*. (*A*) Using multiple sequence alignment, a 255-bp element, *ECR5*, was identified 62 kb downstream of *Sost* transcriptional start site. (*B*) Two TG constructs were used to generate TG mice, *ECR5L* and *3XECR5*. (*C–F*) *ECR5L* expressed *LacZ* in the entire mouse neonate skeleton. Here we show representative images of forelimbs (*C*), hindlimbs (*D*), ribs (*E*), and head (*F*). Lower expression was observed in the calvaria (ca) relative to the mandible (ma). Nonskeletal tissues expressing *LacZ* included the thoracic vasculature (red arrow) (*E*) and the kidney (*G*). At higher resolution, in the calvaria, *ECR5L* (*H*), *3XECR5* (*I*), and *LacZ* expressed from the endogenous mouse *Sost* locus (*J*), marked the osteocytes.

***Mef2C* is Required for *ECR5*-mediated *Sost* Expression in Osteocytes.** Comparative sequence and transcription factor binding site analysis predicted a Mef2 binding site within the *ECR5* element, and this element was shown to be essential for *ECR5* activity in vitro (12). To determine whether Mef2C is required for *ECR5*-mediated transcriptional activation of *Sost* in vivo, we compared *LacZ* expression from either the *ECR5*^{LacZ} or the *Sost*^{LacZ} allele to that of animals where the *Mef2C* gene has also been removed in osteoblasts and osteocytes with a *Col1-Cre* TG (15). This *Col1-Cre* TG is expressed in both osseous and nonosseous tissues: embryonically in the head and limbs, and postnatally in the skeletal system, predominantly in osteoblasts and osteocytes (16). In femora and calvaria, the *LacZ* expression from *ECR5*^{LacZ} was abolished in the absence of *Mef2C* (Fig. 2 *A*, *B*, *E*, and *F*). Similarly, in the femurs of *Sost*^{LacZ} mice, >95% of osteocytes positive for *Sost* did not express *LacZ* when *Mef2C* was deleted (Fig. 2 *C* and *D*). A significant reduction was also observed in calvaria; however, a larger number of *Sost*-positive cells were retained than in the femur (Fig. 2 *G* and *H*).

We also examined *Mef2C* and *Sost* expression in cortical bone of WT and *Mef2C*^{cKO}*; Col1-Cre*. We found *Mef2C* mRNA levels to be reduced by ~70% (Fig. S1*A*) and *Sost* by ~50% (Fig. S1*B*) in *Mef2C*^{cKO}*;Col1-Cre* relative to WT controls. Growth plate chondrocytes robustly expressed Mef2C protein in WT and the expression was unchanged in the *Mef2C*^{cKO}*;Col1-Cre* (Fig. 3 *A* and *E*). Excision of *Mef2C* by *Col1-Cre* eliminated Mef2C protein expression in most osteoblasts and osteocytes relative to WT (Fig. 3 *B*, *C*, *F*, and *G*); particularly on the periosteal surface, all osteoblasts were negative for Mef2C in *Mef2C*^{cKO}*;Col1-Cre* (Fig. 3*F*). The same bone regions that failed to express Mef2C downregulated *Sost* expression, primarily in osteocytes (Fig. 3 *D* and *H*). These results support a model where *ECR5* directs gene expression in osteocytes, and this *ECR5*-dependent expression requires Mef2C (Fig. 2 *B* and *F*). Similarly, Mef2C is required for the majority of mouse *Sost* expression in these cells (Fig. 2 *D* and *H*).

***ECR5*^{KO} Mice Have Increased Bone Mass.** To determine whether deleting *ECR5* causes VB, we made *ECR5*^{KO} mice (Fig. 4 *A–B*). KO mice did not differ in size or weight from their same-sex control littermates, and no overt defects were noted at birth or throughout their lives. At 6 mo of age, microscale computed tomography (μCT) analysis of distal femur and lumbar area (L4) showed that trabecular bone volume fraction (BV/TV) in *ECR5*^{KO} was 41% ($P < 0.000001$) higher than WT (Fig. 4*G*). *ECR5*^{KO} had significantly higher connectivity density (Conn. D., Fig. 4*C*), trabecular number (Tb.N., Fig. 4*D*), and lower trabecular separation (Tb. Sp., Fig. 4*F*), and structure model index (SMI; Fig. 4*H*) compared with WT controls. In the trabecular bone compartment, a significant increase in osteoblast surface (Ob.S) and no significant change in osteoclast surface (Oc.S) was observed. We did observe a significant difference in osteoclast surface to bone surface ratio in both *Sost*^{KO} and *ECR5*^{KO} mice.

Bone formation (BFR/TV, Table 1) in *ECR5*^{KO} mice was significantly increased for trabecular bone (more than twofold in *ECR5*^{KO} relative to approximately threefold in *Sost*^{KO}) at the distal femur. Bone formation was also stimulated at the endocortical surface of the femur midshaft in *Sost*^{KO}, but not in

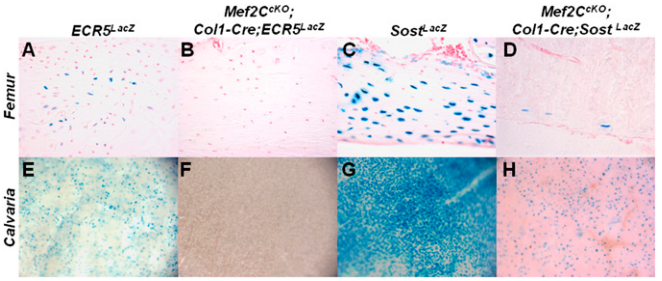

Fig. 2. *Mef2C* is required for *ECR5*-dependent *Sost* expression, in vivo. $ECR5^{LacZ}$ transgenic mice that were also mutant for *Mef2C* did not express *LacZ* in the femur (*B*) or calvaria (*F*) relative to the $ECR5^{LacZ}$ controls (*A* and *E*). Similar results were obtained in $Mef2C^{cKO}$; *Col1-Cre*; $Sost^{KO}$ double knockout animals, where *LacZ* expression was dramatically reduced in the femur (*D*) and calvaria (*H*) relative to $Sost^{LacZ}$ controls (*C* and *G*).

$ECR5^{KO}$ mice, as demonstrated by femoral cortical bone morphology via μCT analysis: Bone area fraction (BA/TA 68.9%) was significantly increased in $Sost^{KO}$ ($P < 1 \times 10^{-10}$), compared with 47.5% in $ECR5^{KO}$ and 46.2% in WT (Fig. 4*E*). Consistent results were obtained through histomorphometric characterization of the cancellous bone compartment at the distal femurs, supporting a HBM phenotype in $ECR5^{KO}$ mice due to elevated bone formation rates (Table 1). In humans, the hyperostosis phenotype in VB disease has been described to be significantly milder than those for sclerosteosis (10). Consistent with the human data, we found the $ECR5^{KO}$ mice to have a significant increase in bone mass (BV/TV, more than twofold, 104% increase, $P < 0.001$), which is less dramatic than in $Sost^{KO}$ (more than threefold, 265% increase, $P < 1 \times 10^{-11}$); therefore, *ECR5* contributes to the VB phenotypes found in the human disease.

***ECR5* Is Necessary for Robust Osteocyte *Sost* Expression in Mice.** *Sost* primarily marked periosteal/cortical and trabecular osteocytes, consistent with its known expression (Fig. S2). No *Sost* expression was detected in proliferating or hypertrophic chondrocytes. $ECR5^{KO}$ expressed *Sost* in a significantly lower percentage of osteocytes (Fig. 4*J*) relative to WT (Fig. 4*I*). To determine the number of osteocytes expressing Sclerostin ~1000 matrix-embedded osteocytes were examined per genotype. Of the 1071 WT osteocytes, 693 (63.4%) expressed Sclerostin (Fig. 4 *I* and *K*). Of the 984 examined $ECR5^{KO}$ osteocytes, 425 (43.11%) were positive for Sclerostin (Fig. 4 *K* and *J*); 32% less positive ($P < 0.02$) $ECR5^{KO}$ osteocytes relative to WT. We found no changes in *Sost* expression in $ECR5^{KO}$ mice relative to WT in kidney, brain, or liver (Fig. S3). These data indicate that deleting *ECR5* reduces the probability that an osteocyte will express high levels of *Sost*, which quantitatively reduces *Sost* expression by ~50% (Fig. S1*B*). This reduction is sufficient to boost bone formation and cause HBM consistent with VB phenotypes.

Mef2C Inactivation in Bone Causes HBM Due to Elevated Bone Formation. We next examined whether targeting *Mef2C* in osteoblasts/osteocytes phenocopies $ECR5^{KO}$ and causes HBM in mice. $Mef2C^{cKO}$;*Col1-Cre* mice were born at normal Mendelian ratios and were indistinguishable from their control littermates at birth. After weaning, these mice were slightly smaller, and their tails displayed swelled protrusions due to increased ossification. Analysis of $Mef2C^{cKO}$;*Col1-Cre* femora and lumbar vertebrae by μCT revealed that osteoblast inactivation of *Mef2C* results in HBM. In every parameter measured (Fig. 5 *A*–*F*), the absolute numbers were highly similar to those determined for $ECR5^{KO}$. $Mef2C^{cKO}$;*Col1-Cre* mice had significantly increased Connectivity Density (Fig. 5*A*), BV/TV (Fig. 5*E*), and decreased SMI (Fig. 5*F*) relative to WT controls, and similar to $ECR5^{KO}$, did not display a significant difference in the trabecular thickness (Fig. 5*C*). BV/TV was increased ~twofold in $Mef2C^{cKO}$;*Col1-Cre* mice (Fig. 5*E*), highly similar to the $ECR5^{KO}$ (Fig. 4*G*).

To determine the cellular mechanism by which the HBM phenotype is generated in $Mef2C^{cKO}$;*Col1-Cre* mice, we examined the cancellous bone compartment of the distal femurs of 6-mo-old male mice using dynamic histomorphometry. Similar to $ECR5^{KO}$ and $Sost^{KO}$, $Mef2C^{cKO}$;*Col1-Cre* mice also displayed a slight decrease in the osteoclast surface to bone surface ratio; however, this difference was not significant. We also observed a significant increase in the mineral apposition rate (MAR) and the bone formation rate (BFR/TV, Table 1), supporting that the removal of *Mef2C* in osteoblasts and osteocytes phenocopies VB (Fig. 5*G*). Recently, it has been reported that $Mef2C^{cKO}$; *Dmp1-Cre* mice display HBM; however, this phenotype was shown to be driven primarily by a reduction in osteoclast activity (19). To further examine whether reduced osteoclast activity in $Mef2C^{cKO}$;*Col1-Cre* contributes to the HBM phenotype, we measured CTX-1 and RANKL serum levels but found no significant differences between $Sost^{KO}$, $ECR5^{KO}$, and $Mef2C^{cKO}$;*Col1-Cre* mice and WT (Fig. S4). Furthermore, we examined the expression of activated β-catenin in the femurs of WT, $Sost^{KO}$, and $Mef2C^{cKO}$; *Col1-Cre* mice and found significantly elevated levels of β-catenin in both $Sost^{KO}$ and $Mef2C^{cKO}$;*Col1-Cre* mice, consistent with an up-regulation of Wnt signaling as a shared mechanism for the HBM in these genetically distinct mice (Fig. S5).

Discussion

Until recently, members of the Mef2 family of transcriptional factors (Mef2A–D) have only been described as contributors to muscle and cardiovascular function (15, 20). In 2007, Arnold et al. reported that Mef2C functions as an early regulator of chondrocyte hypertrophy (14) and showed that Mef2C indirectly controls endochondral bone formation (14). They also reported

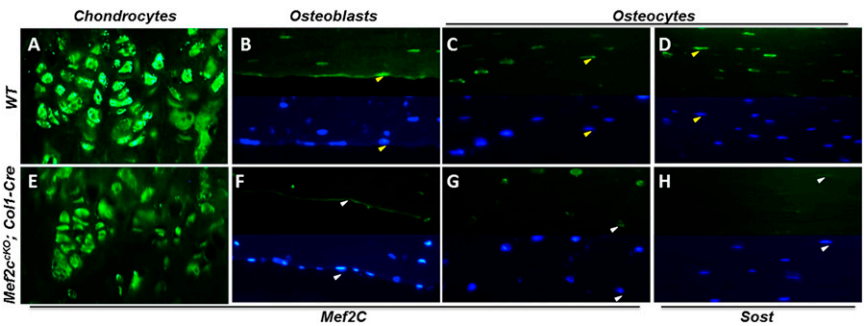

Fig. 3. $Mef2C^{cKO}$;*Col1-Cre* mice have reduced *Mef2C* and *Sost* bone expression. Mef2C protein expression is unchanged in chondrocytes (*A* and *E*). On the periosteal surface, most osteoblasts were positive for Mef2C in the WT (*B*; positive cells are marked by yellow arrows) and this expression was absent in $Mef2C^{cKO}$;*Col1-Cre* (*F*; negative cells are marked by white arrows). Fewer cortical osteocytes expressed Mef2C in $Mef2C^{cKO}$;*Col1-Cre* (*G*; white arrows point to Mef2C negative cells) relative to WT (C, yellow arrows point to Mef2C positive cells). A significant reduction in Sost-positive cortical osteocytes was also observed in $Mef2C^{cKO}$;*Col1-Cre* (*H*; white arrows mark Sost negative cells) relative to WT control (D; yellow arrows mark Sost-positive cells). In *B*–*D* and *F*–*H*, *Upper* is the Mef2C protein signal in the green channel, and *Lower* is the same image showing the cell nuclei (blue channel/DAPI); arrows point to the same cells visualized in the green and blue channel.

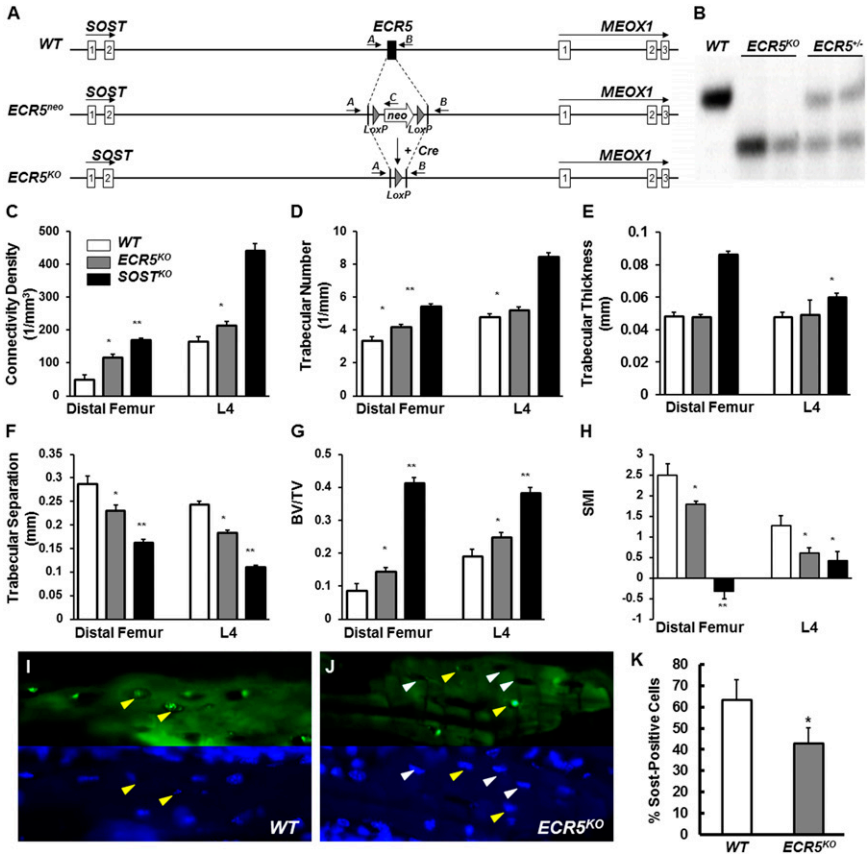

Fig. 4. *ECR5*^{KO} mice have HBM due to reduced number of Sost-expressing osteocytes. *ECR5* was replaced by a neo cassette, which was subsequently removed by *Cre* recombinase to generated *ECR5*^{KO} mice (*A*). *ECR5* targeting was confirmed by Southern blot (*B*). μCT analysis showed significant differences between *ECR5*^{KO} mice and WT control littermates (*C–H*) consistent with *ECR5*^{KO} mice having HBM. Fewer osteocytes expressed *Sost* in *ECR5*^{KO} mice (*L*) compared with WT (*I*); (*Upper*) protein signal (green channel); (*Lower*) the same section visualizing nuclei with DAPI (blue channel). Quantitative assessment of the number of cortical osteocytes expressing *Sost* in *ECR5*^{KO} relative to WT identified a ~30% reduction in *Sost*-positive cells, in *ECR5*^{KO} mice (*K*). Yellow arrows point to Sost-positive cells; white arrows point to Sost-negative osteocytes.

that *Mef2A*, *-C*, and *-D* are expressed in the emerging endochondral bone, in the late embryonic spongiosa (14). Subsequently, we showed that *Sost* expression is modulated by PTH through a Mef2 responsive element, present in the distal *ECR5 Sost* enhancer (12). The results of the study presented here reveal the following insights into the molecular basis of transcriptional regulation of *Sost* in bone: (*i*) *ECR5* is sufficient to drive tissue-specific expression in osteoblasts and osteocytes in vivo (Fig. 1*J*). (*ii*) *SOST* promoter is not required for neonatal expression of *ECR5*-dependent TGs, but is needed for high levels of TG expression in adult osteocytes (Fig. 2*A* vs. 2*C* and 2*E* vs. 2*G*). (*iii*) In the absence of *ECR5* ~30% less osteocytes express Sost (Fig. 5). (*iv*) *ECR5*^{KO} mice have HBM due to elevated bone formation rates resembling VB phenotypes (Fig. 4 *E–J*). (*v*) Mef2C is important in osteocytes for the activity of *ECR5*-dependent *Sost* transcription (Fig. 2*B*, *D*, *F*, and *H*). (*vi*) *Mef2C* deletion from osteoblasts and osteocytes yields HBM and increased bone formation, and displays bone parameters that are similar to *ECR5*^{KO} (Fig. 5 *A–F*), suggesting that Mef2C is the main transcriptional regulator of *ECR5*-dependent *Sost* expression.

Although several regulatory sequences have been characterized and shown to have tissue-specific activity in bone, such as *Col1a1(3.6)* (21, 22) and *Dmp1* (23, 24) the regulatory sequences in these constructs were derived from promoter proximal regions only. *ECR5* represents a distal enhancer that has osteoblast- and osteocyte-specific activity in vivo and is located ~62 kb away from the *Sost* transcriptional start site. *ECR5* is located in the VB region that is deleted from both alleles in VB, and the evidence we present indicates that the human phenotypes are, in part, dependent on the absence of *ECR5* and its interaction with the *SOST* promoter; we also show that *ECR5*^{KO} recapitulates VB in mice. Currently, there is only one other report of a distal transcriptional enhancer: the *RankL* distal regulatory enhancer (*DCR*) that affects bone mass. When deleted, *DCR* caused HBM due to reduced osteoclast activity, leading to a lower rate of bone remodeling similar to that observed in humans and mice with hypoparathyroidism (25, 26).

Because Sost is an inhibitor of an anabolic pathway, there is great interest in elucidating how *Sost* is regulated transcriptionally and posttranslationally, since modulating *Sost* levels has profound consequences downstream of Wnt signaling ranging from promoting bone formation (*Sost* deficiency) (4, 27) to accelerating bone loss (*Sost* overexpression) (7, 28), to enhancing bone repair (29). Here, we provide genetic evidence that Mef2C is important in bone for transcriptional activation of *Sost* in osteocytes, and hence functions as an upstream regulatory protein and modulator of Wnt signaling. In addition to *Sfrp2/3* (19), *Sost* represents a Mef2C transcriptional target in bone; therefore, other Mef2C-dependent transcripts will likely be found in osteoblasts and osteocytes. It is also likely that, through its known corepressor partners, the type II HDAC proteins (14, 20), Mef2C may also serve as a key intermediary in the transmission of extracellular signals to the genome in bone. Further studies of Mef2C-Sost-Wnt signaling axis are likely to reveal basic mechanisms of bone formation and homeostasis, and it should be possible to modulate complex metabolic phenotypes through the manipulation of Sost and Mef2C activities in animal models.

Materials and Methods

Generation of ECR5^{KO}, ECR5L, 3XECR5, and compound Mice. A 338-bp *ECR5* region (101782666-101782996; chr 11) was replaced with a floxed Neo cassette using Velocigene (30) and homologous recombination (31–33) in BAC RP23_252b10. The modified BAC was digested with *SgrA1* and electroporated into ES line F1H4 (C57BL/6–129SvJ hybrid). Targeted ES cell clones were identified using Loss of Allele assay and verified by Southern blot. Two clones (VG1369B-C4/VG1369B-D2) were used to generate mice; both lines had the same HBM phenotype. *ECR5L* and *3XECR5* were PCR amplified

Table 1. Bone phenotying based on histomorphometric indices in the cancellous bone compartment of the distal femurs of 6-mo-old *ECR5*^{KO}, *Sost*^{KO}, and *Mef2C*^{cKO};*Col1-Cre* male mice compared with WT controls

Histomorphometric index	WT	*ECR5*^{KO}	% change	*Sost*^{KO}	% change	WT	*Mef2C*^{cKO}	% change
BV/TV	7.79 ± 4.02	15.894 ± 5.833*	+104	28.45 ± 2.79*	+265	0.127 ± 0.02	0.201 ± 0.05*	+58
BS/BV	70.90 ± 20.54	48.86 ± 12.54*	−31	39.89 ± 4.82*	−44	56.72 ± 9.92	40.39 ± 7.68*	−29
Tb.Dm (Plate)	30.33 ± 8.39	43.82 ± 12.57*	+44	50.85 ± 6.77*	+68	—	—	—
Tb.N (Plate)	2.53 ± 1.16	4.26 ± 1.67*	+68	5.63 ± 0.94*	+122	—	—	—
Tb.Sp (Plate)	438.3 ± 211.7	222.6 ± 83.80*	−49	131.81 ± 29.82*	−70	—	—	—
Tb.Dm (Rod)	—	—	—	—	—	0.072 ± 0.010	0.097 ± 0.02*	+35
Tb.N (Rod)	—	—	—	—	—	5.652 ± 0.87	5.299 ± 0.81	−6
Tb.Sp (Rod)	—	—	—	—	—	0.108 ± 0.02	0.086 ± 0.01*	−20
Ob.S	2.62 ± 1.11	5.956 ± 1.89*	+127	6.143 ± 1.68*	+134	1.402 ± 1.55	3.326 ± 4.40	+137
Ob.S/BS	14.42 ± 3.93	17.730 ± 6.54*	+23	17.16 ± 2.62	+19	0.130 ± 0.15	0.046 ± 0.02	−65
Oc.S	1.64 ± 0.76	1.404 ± 0.364	−14	1.623 ± 0.38	−1	1.743 ± 1.25	1.219 ± 0.73	−30
Oc.S/BS	8.92 ± 3.29	4.426 ± 1.87*	−50	4.608 ± 0.89*	−48	0.067 ± 0.04	0.049 ± 0.02	−27
MAR (μm/d)	2.06 ± 0.36	2.634 ± 0.324*	+28	2.938 ± 0.165*	+42	0.981 ± 0.15	1.368 ± 0.33*	+39
BFR/BS	0.79 ± 0.19	1.188 ± 0.40*	+50	1.035 ± 0.28	+31	0.073 ± 0.02	0.108 ± 0.13	+48
BFR/BV	56.29 ± 23.36	59.89 ± 32.58	+6	40.062 ± 7.96	−29	3.027 ± 1.46	2.829 ± 1.66	−7
BFR/TV	3.87 ± 1.41	8.371 ± 2.84*	+116	11.46 ± 2.57*	+196	0.306 ± 0.12	0.736 ± 0.22*	+141

Data represent mean ± SD for parameters measured. Group size n = 5–10. *P < 0.05. BFR, bone formation rate; BS, bone surface; BV, bone volume; MAR, mineral apposition rate; Ob.S, osteoblast surface; Oc.S, osteoclast surface; Tb.Dm, trabecular diameter; Tb.N, trabecular number; Tb.Sp, trabecular separation; TV, total volume; —, no measurements were conducted.

from human genomic DNA using 5′-GCCAGTCTACTGCCATTGTCC-3′ 5′-GGGCAGAGATTTCTAGGGGTG-3′ and 5′-AATTCTAGCCACTCCCAGGCA-3′ 5′-AATTCGGCTCCCCCTCATGGCTGGT-3′ primer sets, respectively, and cloned into pCR2.1 vector. *ECR5L* was cloned into β-*globin LacZ* vector (gift from M. Nobrega, University of Chicago, Chicago, IL), and three copies of *ECR5*s were cloned in combination with the human SOST promoter we described (7) and topazGFP (gift from D. Rowe, University of Connecticut, Farmington, CT). Plasmid DNA was prepared and injected to generate TG mice as described (34). Pups were genotyped by PCR.

Sost^{KO} mice (*Sost*$^{tm1(KOMP)Vlcg}$) were generated by a *LacZ* replacement of the entire *Sost* ORF. *ECR5*^{LacZ} or *Sost*^{KO} mice were mated to the described *Mef2C*^{cKO} (15) and *Col1-Cre* transgenic mice (16) to generate *Mef2C*^{cKO};*Col1-Cre; ECR5*^{LacZ} and *Mef2C*^{cKO};*Col1-Cre*; *Sost*^{KO} mice. Genotyping was carried out by PCR. All animal experiments were carried out in accordance with

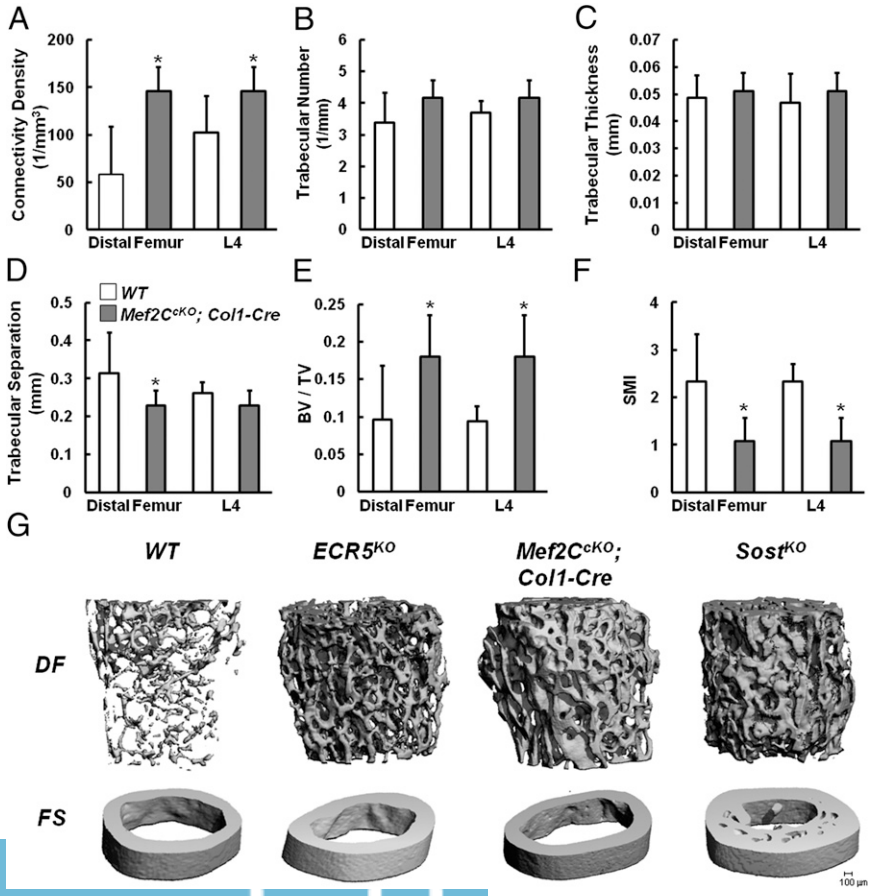

Fig. 5. *Mef2C*^{cKO};*Col1-Cre* mice have HBM. μCT analysis of *Mef2C*^{cKO};*Col1-Cre* mice showed significant differences between *Mef2C*^{cKO};*Col1-Cre* mice and WT control littermates (*A–F*) consistent with *Mef2C*^{cKO};*Col1-Cre* mice having HBM. *Mef2C*^{cKO};*Col1-Cre* mice had significantly increased connectivity density (*A*), bone volume/total volume ratio (BV/TV) (*E*), and significantly decreased trabecular separation in the distal femur (*D*) and SMI (*F*). No significant differences were observed in trabecular number (*B*) or thickness (*C*) or lumber trabecular separation (*D*). Quantitatively and qualitatively, the bones of *Mef2C*^{cKO};*Col1-Cre* mice had higher BMD than WT and less than *Sost*^{KO} and were indistinguishable from *ECR5*^{KO} mice (*G*).

guidelines set by the Institutional Animal Care and Use Committees at University of California, Berkeley, and Lawrence Livermore National Laboratory.

μCT and Histomorphometry. Distal femurs, midfemoral cortical bone, and lumbar (L4) vertebrae were scanned using VivaCT-40 and μCT35 (Scanco Medical) with an isotropic voxel size at 10 or 6 μm. For the metaphysic trabecular bone in distal femur, transverse CT slices were evaluated in the region starting 0.1mm proximal to the growth plate and extending 2mm proximally. Trabecular bone was separated from cortical bone with manually drawn contour lines, and trabecular bone volume fraction (BV/TV, %), trabecular thickness (Tb.Th, mm), trabecular number (Tb.N, mm^{-1}), trabecular separation (Tb.Sp, mm), connectivity density (ConnD, $1/mm^3$), and structure model index (SMI) were determined (SMI quantifies the characteristic form of a three-dimension structure as an index of plates or rods in the bone composition). For the femoral midshaft cortical bone, total cross-sectional area (bone plus bone marrow area) (TA, mm^2), cortical bone area (BA, mm^2), bone marrow area (MA, mm^2), and bone area fraction (BA/TA, %) were calculated.

Bone Histomorphometry. Bone histomorphometry was performed using semiautomatic image analysis (Bioquant Image Analysis) as described (36).

Sost-Positive Cell Scoring. Two animals, 16 slide sections, 250 cells per scoring for up to ~1,000 cells per genotype were examined. Slides were imaged, encompassing the entire mineralized area of the section. Cells were scored as positive if both DAPI and Sost immunostain were present, negative if DAPI was present without any evidence of immunostain. Percentages (% positive) were calculated for each replicate of 250 cells, and compared using Student's paired *t* test. Data are expressed as an average % positive of all replicates + SD.

ACKNOWLEDGMENTS. We thank Dr. Schwarz for providing the *Mef2C*^{cKO}; and Deepa Murugesh, Cindy Thomas, and Salustra Urbin for technical assistance with animal breeding, tissue collection, and sample preparation. G.G.L. and N.M.C. were supported by NIH Grants HD47853 and DK075730; D.C.G. was supported by NIH Grants DK075730 and AR057547. This work performed under the auspices of the US Department of Energy by Lawrence Livermore National Laboratory under Contract DE-AC52-07NA27344.

1. Yadav VK, Ducy P (2010) Lrp5 and bone formation: A serotonin-dependent pathway. *Ann N Y Acad Sci* 1192:103–109.
2. Gong Y, et al.Osteoporosis-Pseudoglioma Syndrome Collaborative Group (2001) LDL receptor-related protein 5 (LRP5) affects bone accrual and eye development. *Cell* 107: 513–523.
3. Cui Y, et al. (2011) Lrp5 functions in bone to regulate bone mass. *Nat Med* 17: 684–691.
4. Li X, et al. (2008) Targeted deletion of the sclerostin gene in mice results in increased bone formation and bone strength. *J Bone Miner Res* 23:860–869.
5. Brunkow ME, et al. (2001) Bone dysplasia sclerosteosis results from loss of the SOST gene product, a novel cystine knot-containing protein. *Am J Hum Genet* 68:577–589.
6. Balemans W, et al. (2001) Increased bone density in sclerosteosis is due to the deficiency of a novel secreted protein (SOST). *Hum Mol Genet* 10:537–543.
7. Loots GG, et al. (2005) Genomic deletion of a long-range bone enhancer misregulates sclerostin in Van Buchem disease. *Genome Res* 15:928–935.
8. Van Wesenbeeck L, et al. (2003) Six novel missense mutations in the LDL receptor-related protein 5 (LRP5) gene in different conditions with an increased bone density. *Am J Hum Genet* 72:763–771.
9. Babij P, et al. (2003) High bone mass in mice expressing a mutant LRP5 gene. *J Bone Miner Res* 18:960–974.
10. Balemans W, et al. (2002) Identification of a 52 kb deletion downstream of the-SOST gene in patients with van Buchem disease. *J Med Genet* 39:91–97.
11. Staehling-Hampton K, et al. (2002) A 52-kb deletion in the SOST-MEOX1 intergenic region on 17q12-q21 is associated with van Buchem disease in the Dutch population. *Am J Med Genet* 110:144–152.
12. Leupin O, et al. (2007) Control of the SOST bone enhancer by PTH using MEF2 transcription factors. *J Bone Miner Res* 22:1957–1967.
13. Loots GG, et al. (2012) TGF-β regulates sclerostin expression via the ECR5 enhancer. *Bone* 50:663–669.
14. Arnold MA, et al. (2007) MEF2C transcription factor controls chondrocyte hypertrophy and bone development. *Dev Cell* 12:377–389.
15. Lin Q, Schwarz J, Bucana C, Olson EN (1997) Control of mouse cardiac morphogenesis and myogenesis by transcription factor MEF2C. *Science* 276:1404–1407.
16. Liu F, et al. (2004) Expression and activity of osteoblast-targeted Cre recombinase transgenes in murine skeletal tissues. *Int J Dev Biol* 48:645–653.
17. Lakso M, et al. (1996) Efficient in vivo manipulation of mouse genomic sequences at the zygote stage. *Proc Natl Acad Sci USA* 93:5860–5865.
18. Gardner JC, et al. (2005) Bone mineral density in sclerosteosis; affected individuals and gene carriers. *J Clin Endocrinol Metab* 90:6392–6395.
19. Kramer I, Baertschi S, Halleux C, Keller H, Kneissel M (2012) Mef2c deletion in osteocytes results in increased bone mass. *J Bone Miner Res* 27:360–373.
20. Potthoff MJ, Olson EN (2007) MEF2: A central regulator of diverse developmental programs. *Development* 134:4131–4140.
21. Bogdanovic Z, et al. (1994) Upstream regulatory elements necessary for expression of the rat COL1A1 promoter in transgenic mice. *J Bone Miner Res* 9:285–292.
22. Zha L, et al. (2008) Collagen1alpha1 promoter drives the expression of Cre recombinase in osteoblasts of transgenic mice. *J Genet Genomics* 35:525–530.
23. Kalajzic I, et al. (2004) Dentin matrix protein 1 expression during osteoblastic differentiation, generation of an osteocyte GFP-transgene. *Bone* 35:74–82.
24. Lu Y, et al. (2007) DMP1-targeted Cre expression in odontoblasts and osteocytes. *J Dent Res* 86:320–325.
25. Kim S, Yamazaki M, Zella LA, Shevde NK, Pike JW (2006) Activation of receptor activator of NF-kappaB ligand gene expression by 1,25-dihydroxyvitamin D3 is mediated through multiple long-range enhancers. *Mol Cell Biol* 26:6469–6486.
26. Galli C, et al. (2008) Targeted deletion of a distant transcriptional enhancer of the receptor activator of nuclear factor-kappaB ligand gene reduces bone remodeling and increases bone mass. *Endocrinology* 149:146–153.
27. Kramer I, Loots GG, Studer A, Keller H, Kneissel M (2010) Parathyroid hormone (PTH)-induced bone gain is blunted in SOST overexpressing and deficient mice. *J Bone Miner Res* 25:178–189.
28. Winkler DG, et al. (2003) Osteocyte control of bone formation via sclerostin, a novel BMP antagonist. *EMBO J* 22:6267–6276.
29. Ominsky MS, et al. (2011) Inhibition of sclerostin by monoclonal antibody enhances bone healing and improves bone density and strength of nonfractured bones. *J Bone Miner Res* 26:1012–1021.
30. Valenzuela DM, et al. (2003) High-throughput engineering of the mouse genome coupled with high-resolution expression analysis. *Nat Biotechnol* 21:652–659.
31. Liu Q, Li MZ, Leibham D, Cortez D, Elledge SJ (1998) The univector plasmid-fusion system, a method for rapid construction of recombinant DNA without restriction enzymes. *Curr Biol* 8:1300–1309.
32. Narayanan K, Williamson R, Zhang Y, Stewart AF, Ioannou PA (1999) Efficient and precise engineering of a 200 kb beta-globin human/bacterial artificial chromosome in E. coli DH10B using an inducible homologous recombination system. *Gene Ther* 6: 442–447.
33. Zhang Y, Buchholz F, Muyrers JP, Stewart AF (1998) A new logic for DNA engineering using recombination in Escherichia coli. *Nat Genet* 20:123–128.
34. Pennacchio LA, et al. (2006) In vivo enhancer analysis of human conserved non-coding sequences. *Nature* 444:499–502.
35. Collette NM, Genetos DC, Murugesh D, Harland RM, Loots GG (2010) Genetic evidence that SOST inhibits WNT signaling in the limb. *Dev Biol* 342:169–179.
36. Ionova-Martin SS, et al. (2011) Changes in cortical bone response to high-fat diet from adolescence to adulthood in mice. *Osteoporos Int* 22:2283–2293.